Sixth International Symposium on Turbulence and Shear Flow Phenomena
Seoul, Korea, 22-24 June 2009

IMPERFECT PHASE SYNCHRONIZATION OF THE WALL TURBULENCE: EXPERIMENTS and DIRECT NUMERICAL SIMULATIONS

Sedat Tardu
LEGI
B.P. 53 X, 38041 Grenoble, Cédex 9, France
Sedat.Tardu@hmg.inpg.fr

ABSTRACT

Instantaneous amplitude and phase concept emerging from analytical signal formulation is applied to the wavelet coefficients of streamwise velocity fluctuations in the buffer layer of a near wall turbulent flow. Experiments and direct numerical simulations show both the existence of long periods of inert zones wherein the local phase is constant. These regions are separated by random phase jumps. These behaviours are reminiscent of phase synchronization phenomena observed in stochastic chaotic systems. The lengths of the constant phase inert (laminar) zones reveal a type-I intermittency behaviour. The observed phenomena are related to the footprint of coherent structures convecting in the low buffer layer that synchronizes the wall turbulence.

INTRODUCTION

The discovery of coherent structures in the early 1960's has profoundly modified our point of view of the wall turbulence structure. The "incoherent" turbulence occupies only 20% of time and space in the inner layer. The coherent part is simpler to understand, since the coherent vortical structures can be identified, and tracked in time and space, and their direct effect on the wall shear and transport of the shear stresses and passive scalar can be clearly determined. The common consensus reached by now points at the existence of quasi-streamwise vortices of diameters typically 10 wall units and located at 20 units from the wall. Their streamwise extend is roughly 300 units, and they generate low and high speed streaks at the wall with a spanwise periodicity of 100 wall units. The sweep and ejection events they generate contribute to the Reynolds shear stress by 80%. The time period of their generation is approximately 100 units also and it depends on the distance from the wall.

Turbulence in general and the wall turbulence in particular can be seen as an infinite dimensional chaotic system. The quasi-periodicity induced by the coherent structures that are convecting in the low buffer layer, should logically lead to the synchronization of the turbulent quantities near the wall. Chaos synchronization is a process wherein chaotic coupled (sub) systems subject to external forcing adjust their time scales resulting in common spatial and temporal dynamics (Boccaletti et al., 2002, Pikovsky et al., 2001). Synchronization can also be defined as the locking between the instantaneous phases of a state variable of the system and the phase of the external periodic force. A rather weak degree of wall turbulence synchronization is expected in a rush environment partially dominated by incoherence. The weaker synchronization between chaotic systems, namely the phase synchronization occurs when the suitably well-defined phases collapse, while the amplitudes remain highly uncorrelated. The noisy synchronization is commonly defined as stochastic synchronization, and the phase locking occurs for random periods of times and is interrupted by random phase slips (Freund et al., 2000; Callenbach et al., 2002). The synchronization of the wall turbulence driven by coherent vortices advecting in the low buffer layer, if it occurs, should be classified in this last category the incoherent part playing the equivalent role of noise.

DEFINITION OF THE INSTANTANEOUS FREQUENCY

Special techniques are necessary to detect the synchronization, which is generally hidden in phase synchronization of chaotic systems and in stochastic synchronization that is further difficult to depict. We apply the instantaneous amplitude and phase concept to the scale decomposed turbulent quantities in the present investigation. The scale decomposition is obtained through wavelet analysis.

Let $\Omega(T_W,t)$ be the wavelet coefficient of the real valued function $u(t)$:

$$\Omega(T_W,t)=\frac{1}{2T_W}\int_{-\infty}^{\infty}u(\tau)\,g\left[\frac{\tau-t}{2T_W}\right]d\tau \qquad (1)$$

where, $a=2T_W$ and t denote respectively the scaling and shift parameters and g is the mother wavelet. The wavelet frequency scale parameter is defined as $k=\frac{2\pi}{T_W}$ hereafter,

in this session. Any signal, moreover the wavelet coefficients $\Omega(k,t)$ may be expressed as:

$$\Omega(k,t)=r(k,t)\cos\left[\int_0^t \omega_i(k,t)\right] \quad (2)$$

where $r(k,t)$ stands for the instantaneous amplitude and $\omega_i(k,t)$ is the instantaneous angular frequency at scale k. The representation (1) is not unique and different characterizations are possible, depending upon the choice of the dual processes. In the Rice canonical representation that is optimum in the sense of minimizing the average rate of the signal envelope, one has:

$$r^2(k,t)=\Omega^2(k,t)+\breve{\Omega}^2(k,t) \quad (3a)$$

by using the Hilbert transform $\breve{\Omega}(k,t)$ of $\Omega(k,t)$, and:

$$\omega_i(k,t)=\frac{\Omega(k,t)\breve{\Omega}'(k,t)-\Omega'(k,t)\breve{\Omega}(k,t)}{r^2(k,t)} \quad (3b)$$

where ' denotes the time derivative. The corresponding optimum carrier frequency equals:

$$\omega_c(k)=\frac{\overline{r^2(k,t)\omega_i(k,t)}}{\overline{r^2(k,t)}} \quad (4)$$

Moreover, the dual of $\Omega(k,t)$ is obviously its Hilbert transform:

$$\breve{\Omega}(k,t)=r(k,t)\sin\left[\int_0^t \omega_i(k,t)dt\right] \quad (5)$$

The instantaneous frequency may also be written as:

$$\omega_i(k,t)=\omega_c(k)+\frac{d\varphi(k,t)}{dt} \quad (6)$$

where $\varphi(k,t)$ is the random phase at scale k. It is straightforward that $\omega_i(k,t)$ governs directly the behavior of $\Omega(k,t)$ near the zero-crossings.

EXPERIMENTS

We used the simplest Haar wavelet in this session. We omit the details here, and simply indicate that quite similar results have been obtained by other mother wavelets such as Mexican hat. The transitions from ejections to sweeps detected by the Haar wavelet at large eddy scales behave as a discontinuous phase frequency shift keying process (Aulin and Sundberg, 1981), with random, yet somewhat coherent and regular periodicity. Fig.1 shows some traces of the phase $\varphi(k^+,t^+)$ and amplitude $r^+(k^+,t^+)$ of the fluctuating streamwise velocity signal u' at $y^+=10$, for the wavelet scale parameter $k^+=0.057$ (corresponding to the wavelet window duration $T_W^+=26$). The optimum angular carrier frequency is $\omega_c^+=0.08$ in this case. It is seen in Fig.1 that the instantaneous phase $\varphi(k,t)$ consists of line segments that are discontinuous at points B and D where random phase jumps occur. The phase increases first at A-B, remains constant during a large period C-D, jumps again and increases at D-F. The constancy of the phase indicates that the instantaneous frequency is sensibly equal to the carrier frequency. The periods like C-D wherein $\omega_i \approx \omega_c$ coincide generally with large amplitudes $r^+(k^+,t^+)$ as clearly seen in Fig.1. Strong ejection-sweeps transitions marking the arrival of coherent structures are, therefore, merely constant phase events. The time intervals as A-B wherein $\varphi(k^+,t^+)$ increases while $r^+(k^+,t^+)$ decreases are reminiscent of apparition of small scales. The slop of A-B is $\frac{d\varphi^+}{dt^+}=\frac{\omega_c^+}{3}$ indicating that $\omega_i(k,t)$ is jumped by a factor 4/3. The jumps in frequency with the *same* fraction of ω_c^+ are often and repetitively observed. It is asked whether this behavior can be partly explained by the multifractal nature of the cascade process or not (Argoul and al., 1989). The epochs as E-F, wherein both the instantaneous phase and the amplitude increase from small values, are presumably related to the arrival of smaller scale active structures.

The occurrence of these long periods is particularly interesting. They refer to the set-up of stochastic synchronization, and appearance of "laminar" periods wherein the instantaneous frequency locks to the mean carrier frequency. The locking frequency corresponding to Fig. 1 is $f_c^+=\omega_c^+/2\pi=0.011$ which is precisely the median ejection frequency at $y^+\approx 15$ where the production reaches its maximum. The physical interpretation of the occurrence of constant phase zones is related to the phase synchronization between the wall turbulent quantities and the forcing imposed by the coherent vortices generated and convecting near the wall. For phase synchronization of coupled chaotic oscillators, as it will be discussed in detail in the following, a very large constant phase locked zone is followed by a very short turbulent stage (the turbulent stage here refers to periods wherein the signal is chaotic according to the terminology used in chaos synchronization). The difference here, is that, not only the duration of phase locked zones is random, but also that the phase *smoothly* fluctuates before sharp increases or phase jumps. Furthermore, zones like A-*B* wherein the phases increase do not exist in the case of coupled chaotic oscillators, that are subject to quiescent periods followed by rapid phase slips. This behavior is due to the stochastic nature of the turbulence that is under the effect of incoherence. When the phase synchronization is perfect the average duration T_l of the phase locking regions separated by successive phase slips scales as:

$$T_l \propto \left|C-C_{ps}\right|^{-\gamma} \quad (7)$$

where C is either the coupling strength or the frequency (wavenumber) of the driving signal. The exponent $\gamma>0$ is $\gamma=1$ in the case of on-off intermittency, and $\gamma=\frac{1}{2}$ for the type I intermittency. The parameter C_{ps} is the critical value of the phase synchronization. It is impossible to observe perfect synchronization in stochastic systems with incoherent turbulence (IT). The phase locked regions are interrupted by IT induced phase slips, and the system does not exhibit infinite "laminar" lengths. We define the occupancy $\Theta=\sum T_{li}/T_{total}$ by the sum of the time-lengths of the laminar zones to the total duration of the data. The

occupancy seen that Θ goes through a well-defined maximum at $k^{*+}=0.25$ and $k^{*+}=0.20$ for respectively u' at $y^+=10$ and the fluctuating wall shear stress τ', and decreases for larger and smaller wavelengths (not shown here). Fig. 2 shows $ln\Theta$ versus $ln\left|k^+-k^{*+}\right|$. It is clearly seen that the type I intermittency with $\Theta \propto \left|k^+-k^{*+}\right|^{-1/2}$ holds reasonably well for $\left|k^+-k^{*+}\right| \geq 0.14$. The type-I intermittency is connected to the saddle-node bifurcation of the locking periods. These points are discussed in more details in Tardu (2008). We will focus on new results in this paper obtained through direct numerical simulations performed in a low Reynolds number turbulent channel flow.

DIRECT NUMERICAL SIMULATIONS

We use a DNS data basis ($\mathrm{Re}_\tau = 180$), multiple scale edge detection (Mallat and Zhong, 1992) and directional Hilbert transforms (Granlund and Knutsson, 1995) together with 2D Hardy wavelets to detect two-dimensional singularities. We consequently extracted information related to the local amplitudes and phases versus the scale, in a manner similar to the section preceding section. Let 2 wavelets defined by:

$$\psi^1(x,z)=\partial\theta(x,z)/\partial x,\ \psi^2(x,z)=\partial\theta(x,z)/\partial z \qquad (8)$$

where, θ is the smoothing function taken as a Gaussian here, while x and z stands respectively for the streamwise and spanwise directions. The wavelet coefficients at scale s are given by:

$$\begin{aligned} {}^sW_1 u(x,z) &= u \otimes {}^s\psi_1(x,z) = s\frac{\partial}{\partial x}(u\otimes {}^s\theta)(x,z) \\ {}^sW_2(x,z) &= u \otimes {}^s\psi_2(x,z) = s\frac{\partial}{\partial z}(u\otimes {}^s\theta)(x,z) \end{aligned} \qquad (9)$$

The local maxima of ${}^sW_i u(x,z)$ correspond to the sharp smoothed gradients of the velocity field, or to the inflection points of the convolution $u\otimes {}^s\theta$. The computations are performed in Fourier domain in practice, and a fast algorithm is available but the details are omitted here. The scale s is not a continuous parameter and varies along the dyadic sequence $2^j_{j\in N}$. The largest scale here is $m=8$. The wavenumber k^+ at a given scale $j=m$ is defined as $k^+=\dfrac{2\pi}{2^m\left(\Delta x^+\Delta y^+\right)^{1/2}}$ where $\Delta x^+=13$ and $\Delta z^+=6$ are the mesh sizes in the streamwise and spanwise directions.

Let us introduce now, ${}^s\breve{W}_1$ and ${}^s\breve{W}_2$ the directional Hilbert transform of the wavelet coefficients. Let $\hat{W}_1(\omega_x,\omega_z)$ denotes the Fourier transform of W_1. The directional Hilbert transform following x is defined as $\hat{\breve{W}}_{1,x}=j\hat{W}sign(\omega_x)$ where $sign(\omega_x)$ is the sign of ω_x and $j=\sqrt{-1}$. The computations are performed in Fourier domain in practice, and a fast algorithm is available but the details are omitted here. The wavelet ψ_1 is then defined in Fourier domain by

$$\psi_1(2\omega_x,2\omega_y)=G(\omega_x)\phi_0(\omega_x)\phi_0(\omega_y)$$

with

$$G(\omega)=4je^{j\omega/2}\sin(\omega/2) \quad \text{and} \quad \phi_0(\omega)=\left[\frac{\sin(\omega/2)}{(\omega/2)}\right]^3.$$

Similar relations hold for ψ_2 and the details can be found in Mala and Zhong (1992).

For the band-pass wavelet transforms at a given scale s, one can define a local amplitude and wavenumber through along the prescribed direction i ($i=1$ and $i=2$ corresponds respectively to the streamwise and spanwise directions):

$${}^sW_i = {}^sA_i\cos\left[\int {}^sk_i\, dx_i\right] \qquad (10)$$

where, the amplitude is:

$${}^sA_i(x,z)=\sqrt{{}^sW_i^2+{}^s\breve{W}_i^2} \qquad (11)$$

The local wavenumber that minimize the space variations of the envelope is given by:

$${}^sk_i=\frac{{}^sW_i\frac{\partial\,{}^s\breve{W}_i}{\partial x_i}-{}^s\breve{W}_i\frac{\partial\,{}^sW_i}{\partial x_i}}{{}^sA_i^2} \qquad (12)$$

The carrier wavenumber is defined by:

$${}^sk_{ci}=\frac{E\left[{}^sA_i{}^2\,k_i\right]}{E\left[{}^sA_i{}^2\right]} \qquad (13)$$

with E standing for spatial averaging. With the introduction of the carrier frequency, one can define a local phase by

$${}^sW_i = {}^sA_i\cos\left[{}^sk_{ic}\ x_i+{}^s\Phi_i\right] \qquad (14)$$

We set the direction $i=1$ hereafter and replace i by the corresponding streamwise direction x. In the streamwise constant phase zones, the local wavenumber obeys to ${}^sk_x(x,z)={}^sk_{cx}$ at a given scale s. Fig. 3 shows the contours of the events defined as the ensemble of points where: $0.9\ {}^sk_{cx}\le {}^sk_x\le 1.1\ {}^sk_{cx}$ and obtained at $y^+=20$. The emerging contours were more regular by using these thresholds, instead of taking ${}^sk_x(x,z)={}^sk_{cx}$ directly, but the results did not change significantly. The spurious zones where the phase is only punctually constant are eliminated. Elongated constant streaky zones exist at each scale, and occupy a large amount of the homogeneous plane as seen in Fig.3. It is clearly seen that at $k^+=0.044$ (Fig. 3b) the constant phase zones are of larger scales than at $k^+=0.178$ (Fig. 3a) although their relative occupations of the whole plane are relatively comparable with respectively 0.23 and 0.17. Their length scales are several times larger than $2\pi/{}^sk_{cx}$, i.e. one wavelength. In order to quantify the space occupied by constant phase events, we define the quantity Θ by dividing the number of constant phase events to the total number of points. Note that this is just the definition of the occupancy already used in Fig. 2 for experimental data. Fig. 4 shows $ln\Theta$ versus $ln\left|k^+-k^{*+}\right|$ with $k^{*+}=0.15$ at which the maximum occupancy occurs.

This value differs only slightly from $k^{*+} = 0.25$ corresponding to experimental u' data at $y^+ = 10$. Type I intermittency clearly occurs for $\left|k^+ - k^{*+}\right| \geq 0.1$. There is also reasonable correspondence between the experimental and DNS data, taking into account the differences in the methodology, the mother wavelets and the detection points.

The local amplitude $A_x(x,z)$ defined through the equation (11) varies slowly in the phase locked zones. We show in Fig. 5 the flatness factor of $A_x(x,z)$ defined in the usual way as to characterize the associated intermittence. The flatness $F_{A'x}$ is computed globally but also separately in the phase varying and phase locked regions, first taking the mean values individually in these zones, and then computing the normalized fourth order moment of the fluctuating amplitudes $A'_x(x,z) = A_x(x,z) - E(A_x)$. It is seen in Fig. 5 that the intermittency of the local amplitude increases with the wavenumber as expected, both globally and in the varying phase zones, the increase being more pronounced in the latter case. In the phase varying zones for instance the flatness reaches values as high as 9 at the highest wavenumber. The amplitude in the phase locked zones, however is significantly less intermittent, $F_{A'x}$ is practically uniform across the whole wavenumber range, it is smaller than the Gaussian value and varies from 1 to 2. This shows that the amplitude in the constant phase zones approach a uniform distribution in the high wavenumber range, and the uniformity of $F_{A'x}$ at large k^+ indicates clearly that the wavelet coefficients oscillate smoothly in the constant phase zones.

Coherent structures near the wall are situated in the low buffer layer concentrated roughly at $\delta^+ = 20$. Let us define an external forcing at the scale 0 by ${}^0\Omega = 2\pi/\delta^+$. That represents the direct effect of coherent vortices convecting near the wall and inducing phase locking of the wall turbulence. Suppose that the forcing acting at the dyadic scale $s = 2^i$ is self-similar and directly of the form ${}^s\Omega = {}^s\Omega/2^i$. The frequency locking between the fluctuating near wall velocity at a given scale and the external forcing occurs when the local wavenumber is of the form ${}^s k_x(x,z)$ frequency is of the form ${}^s k_x = \frac{m}{n}{}^s\Omega$ where m and n are integers (Rosenblum et al., 1996). That reduces to ${}^s k_{cx} = \frac{m}{n}{}^s\Omega$ in terms of carrier wavenumber during the constant phase zones. Fig. 6 shows the ratio ${}^s k_{cx} / {}^s\Omega$ versus k^+. There is quite a reasonable agreement between this simplified theory and the DNS data leading to $m/n = 1/4$.

CONCLUSION

The analytic signal concept is applied to the wavelet coefficients of fluctuating streamwise velocity in the low buffer layer. Automatic separation of different time scales through both the Hilbert transform that freezes the slow variables and the wavelet analysis allows to sort out the hidden phase synchronization. Long quiescent periods of about 100 wall units wherein the phase oscillates around constant values are noticed near the critical scale parameter. The constant phase zones are interrupted by rapid phase jumps. A parallelism is constructed between these behaviors and the stochastic synchronization of chaotic systems that are under the effect of noise, or incoherence as is the case of the near wall turbulence. Both experimental and direct numerical simulation results converge to the more or less similar results. They both reveal the existence of type-I intermittency connected to the saddle-node bifurcation of the locking periods. The occurrence of long quiescent periods of constant phases of the wavelet coefficients is interesting and may be used in some control strategies. The phase jumps in particular are unambiguously well defined near the critical wavelet scale parameter. The long time periods between the jumps annunciate the arrival of active structures. A gain in effectiveness may presumably be achieved if the decision and action stages of active control schemes coincide with these periods. Strategies similar to the chaos control can also be developed on the basis of the results presented here. It is expected that local excitation the wall turbulence near the critical scale parameter improves the efficiency of active control strategies. Tardu and Doche (2007) have shown for instance that a local blowing of frequency near the bursting frequency doubles the efficiency of suboptimal control, and synchronizes the fluctuating wall shear stress over significantly long streamwise distances downstream of local forcing.

REFERENCES

Aulin T., Sundberg C.E.-W., 1981 "Continuous phase modulation" IEEE Trans. Commun, COM-29.

Boccaletti S., Kurths J.,Osipov G. ,Valladeres D.L., Zhou C.S. , 2002 "The synchronization of chaotic systems" *Phys. Rep.*, **366**, 1.

Callenbach L. ,Hanggi P. , Linz S.J., Freund J.A., Schiemansky-Geier L., 2002 "Oscillatory systems driven by noise: Frequency and phase synchronization" *Phys. Rev. E,* **65**, 051110.

Freund J., Neiman A., Schiemansky-Geier L., 2000, "Analytic description of noise induced synchronization" *Europhysics Letters*, **50**, 8.

Granlund G.H., Knutsson H., 1995 "Signal processing for computer vision" Kluwer Academic Publishers, Dordrecht, Boston, London.

Mallat S., Zhong S., 1992, IEEE *Transactions on Pattern Analysis and Machine Intelligence*, 14, 710.

Pikovsky, A.S, Rosenblum, M.G., Kurths J., 2001, "Synchronization. A Universal Concept in Nonlinear Sciences" Cambridge University Press, Cambridge.

Rosenblum M. Pikovsky A.S., Kurths J.,, 1996 "Phase synchronization of chaotic oscillators" *Phys. Rev. Lett*., **76**, 1804.

Tardu S., Doche O., 2007 « Active control effectiveness and synchronization of wall turbulence under localized imposed unsteadiness » *Phys. Fluid*s, 19, 108103-107.

Tardu S., 2008 Stochastic synchronization of the near wall turbulence », *Phys. Fluids* 20, 045105 .

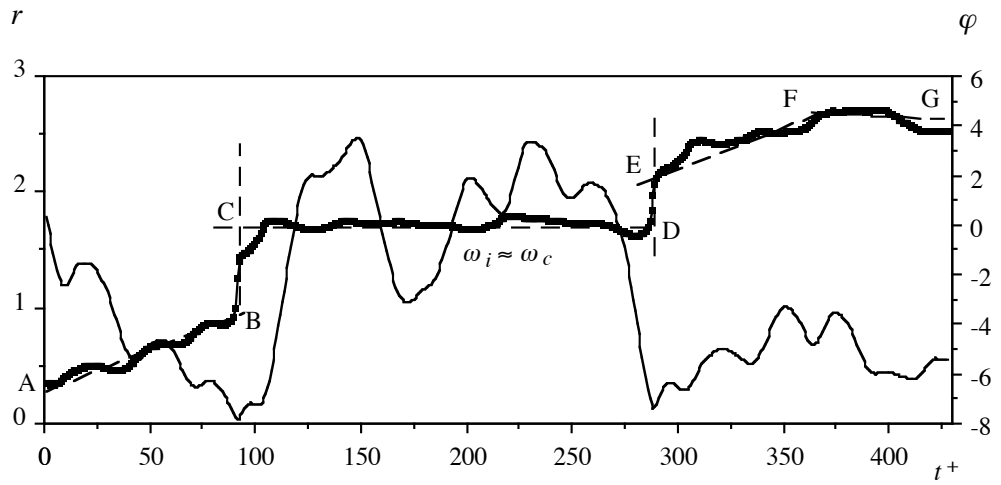

Figure 1: Samples of the instantaneous amplitude (continuous line) and phase (thick line) in radians of the Haar wavelet coefficients of the fluctuating streamwise velocity at $y^+ = 10$ versus time .The scale parameter of the wavelet transform is $k^+ = 0.24$ in wall units.CD: Constant phase zone wherein the instantaneous frequency is equal to the carrier frequency.AB: The phase increases while the amplitude decreases: Apparition of small-scale structures.EF: The phase and amplitude increase simultaneously: Small scale amplitude variations.DE: Phase jump.FG: Constant phase zone.

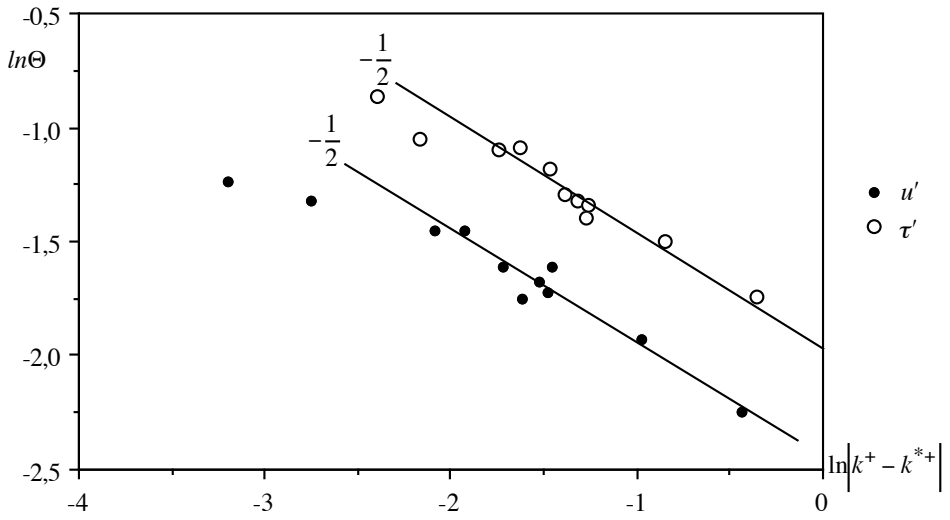

Figure 2: Type-I intermittency of the occupency of phase locked zones. Data are from the velocity fluctuations u'at $y^+ = 10$ and wall shear stress fluctuations τ'.

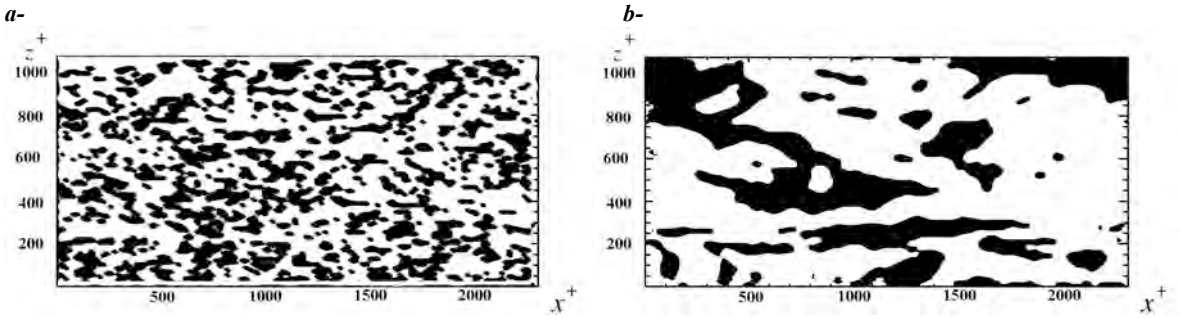

Figure 3: Phase locked zones at $y^+ = 20$ for the wavenumbers $k^+ = 0.178$ (a) and $k^+ = 0.044$ (b).

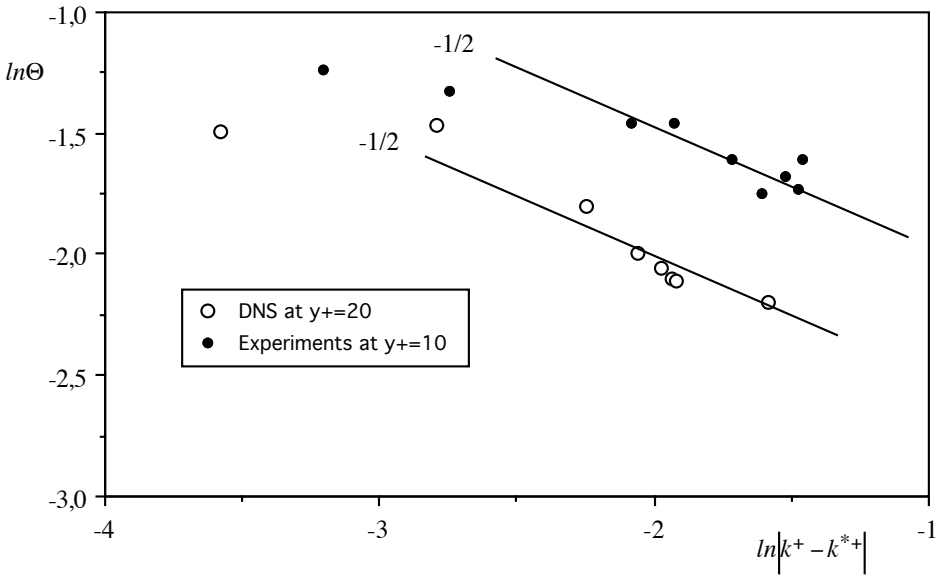

Figure 4: Type I intermittency emerging from dyadic wavelet decomposition of the DNS data at $y^+ = 20$. Comparison with experimental data at $y^+ = 10$.

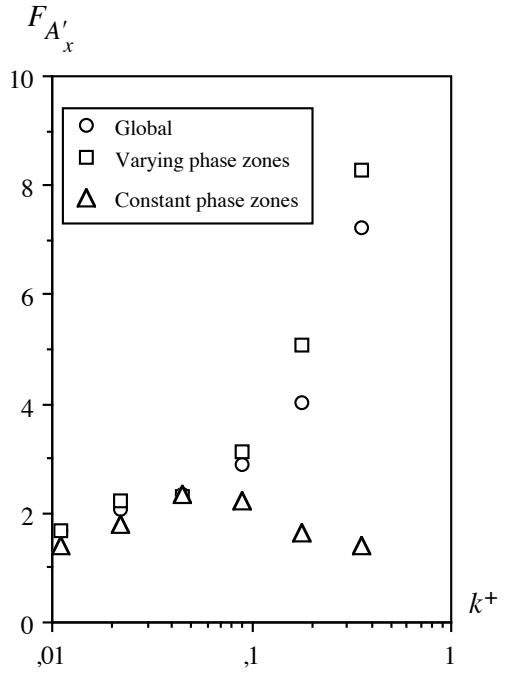

Figure 5: Flatness of the amplitudes.

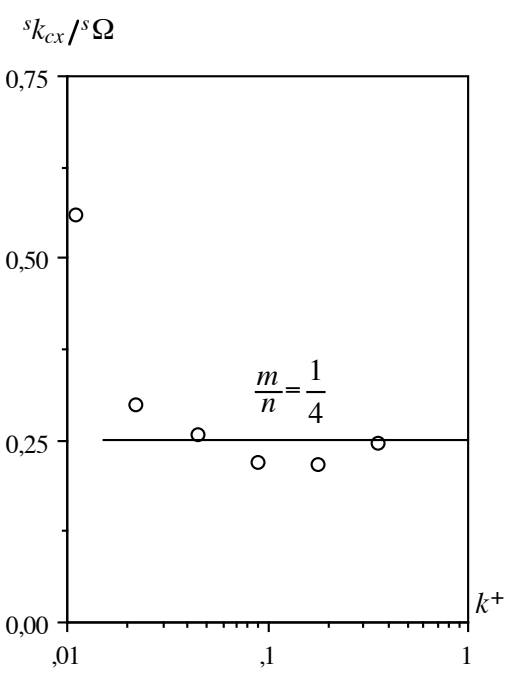

Figure 6: Carrier wavenumber. See the text for details.